Chao, J., Ram, S., Abraham, A., Ward, E. S., and Ober, R. J. Resolution in 3D in multifocal plane microscopy. In *Three-Dimensional and Multidimensional Microscopy: Image Acquisition and Processing XV. SPIE International Symposium on Biomedical and Optics (BiOs),* 6861: 6861-0Q, 2008.

http://dx.doi.org/10.1117/12.763084

Resolution in 3D in multifocal plane microscopy

Jerry Chao[a,b], Sripad Ram[b], Anish V. Abraham[b,c], E. Sally Ward[b] and Raimund J. Ober[a,b]

[a]Department of Electrical Engineering, University of Texas at Dallas, Richardson, TX, USA;
[b]Department of Immunology, University of Texas Southwestern Medical Center, Dallas, TX, USA;
[c]Department of Computer Science, University of Texas at Dallas, Richardson, TX, USA.

ABSTRACT

Using single molecule microscopy, biological interactions can be imaged and studied at the level of individual biomolecules. When characterizing an imaged biological interaction, the distance separating the two participating biomolecules can provide valuable information. Therefore, the resolvability of an imaging setup is of practical significance in the analysis of the acquired image data. Importantly, the resolvability of the imaging setup needs evaluation in the 3D context, since in general biomolecules reside in 3D space within the cellular environment. We recently introduced an information-theoretic 2D resolution measure which shows that the resolution limit due to Rayleigh's criterion can be overcome. This new result predicts that the resolution of optical microscopes is not limited, but rather can be improved with increased photon counts detected from the single molecules. The 2D result was subsequently extended to the 3D context, and the proposed information-theoretic 3D resolution measure can readily be used to determine the resolvability of a conventional single focal plane imaging setup. Here, we consider the 3D resolution measure for a multifocal plane microscope setup, an imaging system which allows the concurrent imaging of multiple focal planes within a specimen. The technique is useful in applications such as the tracking of subcellular objects in 3D. By comparing their 3D resolution measures, we find a two-plane setup to outperform a comparable conventional single-plane setup in resolvability over a range of axial locations for the single molecule pair. Moreover, we investigate and compare the impact of noise on the resolvability of the two setups.

Keywords: 3D resolution measure, Fisher information matrix, Cramer-Rao inequality, multifocal plane microscopy

1. INTRODUCTION

Single molecule microscopy has given investigators the ability to observe and image biological interactions at the level of individual biomolecules within a cellular environment. In the analysis of an imaged interaction, the distance that separates the two closely spaced biomolecules is an important indicator of the nature of the interaction. It is therefore of interest to the microscopist to assess the resolvability of the particular experimental setup used to image the biological specimen.

In a cellular environment, the biomolecules participating in biological interactions are in general situated in 3D space. Therefore, while much research has focused on the 2D resolution problem wherein both interacting molecules are assumed to lie in a plane perpendicular to the optical axis, it is of practical importance to consider the resolution problem in a 3D context. Recently, an information-theoretic 2D resolution measure was proposed which shows that the resolution limit imposed by the widely invoked Rayleigh's criterion can be overcome.[1] This result was subsequently extended to the 3D scenario,[2] and analogous to its 2D counterpart, the proposed information-theoretic 3D resolution measure provides, for a given imaging setup, a lower bound on the accuracy with which the distance separating two single molecules residing in 3D space can be determined. Importantly, this resolution measure predicts that the resolution of optical microscopes is not limited, but in fact can be improved by collecting more photons from the source single molecule pair. For a conventional microscope setup consisting of a single focal plane, this result for the 3D scenario can be applied directly.

Corresponding author: Raimund J. Ober, E-mail: ober@utdallas.edu.

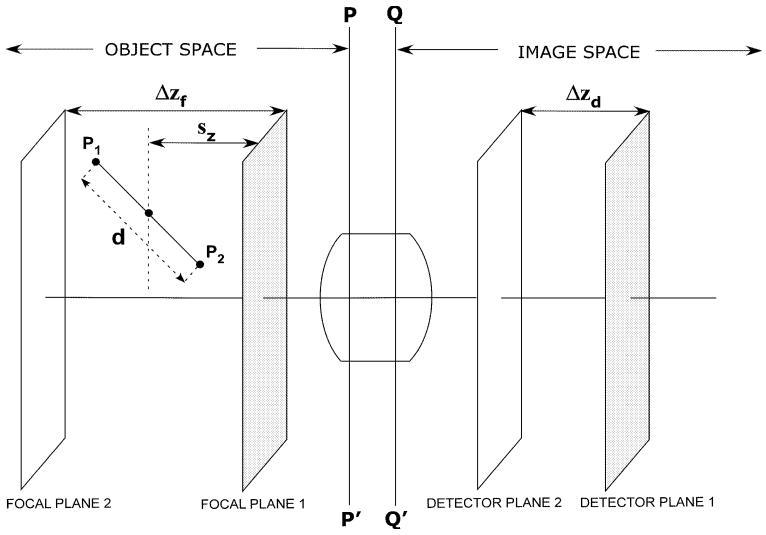

Figure 1. Principle of multifocal plane microscopy illustrated with a two-plane imaging setup. Two detector planes are positioned in the image space at distinct distances from the microscope optics, each having a corresponding focal plane in the object space. Also shown is a pair of single molecules P_1 and P_2 separated by a distance d in 3D space. The midpoint between the two single molecules is located at an axial distance s_z above focal plane 1.

In the current work, we present the 3D resolution measure for a multifocal plane microscope setup.[3] Multifocal plane microscopy is a technique that enables the simultaneous imaging of distinct focal planes within a specimen. Among its useful applications are the 3D localization of single molecules[4] and the visualization of tracks taken by subcellular objects in 3D space.[5] Here we study the 3D resolution measure for a two-plane imaging setup. Specifically, we observe its behavior as a function of the axial position of a single molecule pair. We look at its dependence on the distance separating the two single molecules, as well as its dependence on the orientation of the single molecule pair with respect to the optical axis. Importantly, we compare the 3D resolution measure for the two-plane setup with that for a comparable conventional single focal plane microscope, and observe the axial locations of the single molecule pair for which the two-plane setup yields improved resolvability. Further observation is made of the axial locations of the single molecule pair for which the resolution measure for the two-plane setup is less susceptible than that for the conventional microscope to the deteriorating effect of noise from sources such as cellular autofluorescence and the detector readout process.

2. MULTIFOCAL PLANE MICROSCOPY

Fig. 1 illustrates the principle of multifocal plane microscopy[3] using a two-plane imaging setup. The setup employs two cameras to simultaneously capture images at two distinct focal planes within the specimen in the object space. One camera is positioned at detector plane 1 and takes images of the specimen at focal plane 1. Detector plane 1 can, for instance, be the infinity-corrected detector plane. Similarly, focal plane 1 can be the infinity-corrected standard focal plane. The other camera is situated at detector plane 2 which is closer to the microscope optics than detector plane 1. This camera captures accordingly images of the specimen at focal plane 2 which is above focal plane 1. Simultaneous imaging by the two cameras can be realized by splitting the fluorescence collected by the microscope objective into two light paths using a beam splitter, and by directing each light path to its respective camera.

In comparison, a conventional single focal plane microscope setup would entail a single undivided light path directed to a camera positioned at one of the detector planes.

3. 3D RESOLUTION MEASURE FOR MULTIFOCAL PLANE MICROSCOPY

The 3D resolution measure is defined as the square root of the inverse of the Fisher information matrix $\mathbf{I}(d)$ calculated for the parameter estimation problem wherein the unknown parameter to be estimated from the

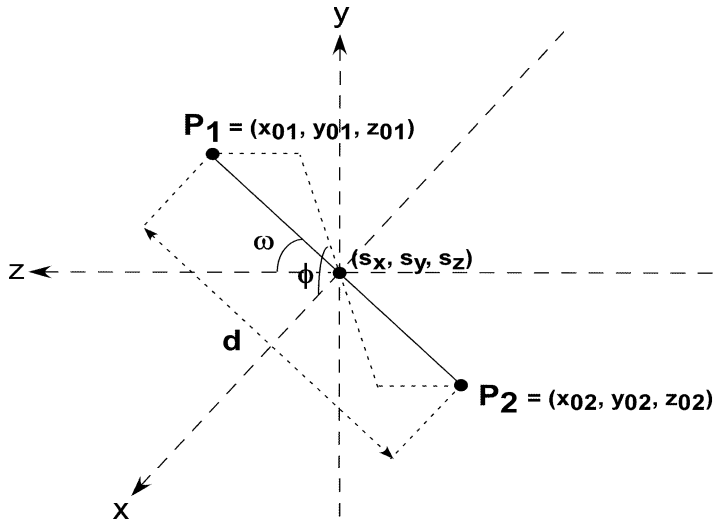

Figure 2. Notation used to describe the 3D location of two single molecules P_1 and P_2 separated by a distance d. The line segment P_1P_2 has its midpoint at (s_x, s_y, s_z), and its orientation in 3D space is given by angles ω and ϕ.

acquired image data is the distance d between two single molecules. According to the Cramer-Rao inequality $Var(\hat{d}) \geq \mathbf{I}^{-1}(d)$, the 3D resolution measure by definition gives a lower bound on the accuracy with which the separation distance d can be estimated by any unbiased estimator $\hat{d}$. For a conventional single focal plane imaging setup, the detailed derivation of the 3D resolution measure can be found elsewhere.[1,6] Here we give only a brief discussion of the single-plane 3D resolution measure as a means of arriving at an expression for the 3D resolution measure for a two-plane imaging setup.

Due to the stochastic nature of the acquired image data, a spatio-temporal random process[7] is used to model the acquired data in a general parameter estimation problem in optical microscopy. We refer to this space-time random process as the image detection process.[6] For a scalar unknown parameter $\theta \in \Theta$, where Θ is the parameter space, the Fisher information matrix for the image data acquired during the time interval $[t_0, t]$ with a pixelated detector is given by

$$\mathbf{I}(\theta) = \sum_{k=1}^{N_p} \frac{1}{\mu_\theta(k,t) + \beta(k,t)} \left(\frac{\partial \mu_\theta(k,t)}{\partial \theta} \right)^2, \tag{1}$$

where $\mu_\theta(k,t) = \int_{t_0}^{t} \int_{C_k} \Lambda(\tau) f_{\theta,\tau}(r) dr d\tau$ denotes the mean of the Poisson-distributed number of photons from the single molecules that is detected at the k^{th} pixel C_k, $\beta(k,t)$ denotes the mean of the Poisson-distributed number of spurious photons due to noise sources such as cellular autofluorescence and scattering that is detected at pixel C_k, and N_p denotes the number of pixels that comprise the detector. The function Λ in the expression for μ_θ is the intensity function of the inhomogeneous Poisson process which models the time points at which photons are detected, and here it is taken to be independent of the unknown parameter θ. The function $f_{\theta,\tau}$ in the same expression is the density function of the independent random variables which model the spatial coordinates at which the photons hit the detector.

If in addition we account for the readout noise due to the detector, then the Fisher information matrix becomes

$$\mathbf{I}(\theta) = \sum_{k=1}^{N_p} \left(\frac{\partial \mu_\theta(k,t)}{\partial \theta} \right)^2 \left(\int_{\mathbb{R}} \frac{\left(\sum_{l=1}^{\infty} \frac{[\nu_\theta(k,t)]^{l-1} e^{-\nu_\theta(k,t)}}{(l-1)!} \cdot \frac{1}{\sqrt{2\pi}\sigma_k} e^{-\frac{1}{2}\left(\frac{z-l-\eta_k}{\sigma_k}\right)^2} \right)^2}{\frac{1}{\sqrt{2\pi}\sigma_k} \sum_{l=0}^{\infty} \frac{[\nu_\theta(k,t)]^{l} e^{-\nu_\theta(k,t)}}{l!} e^{-\frac{1}{2}\left(\frac{z-l-\eta_k}{\sigma_k}\right)^2}} dz - 1 \right), \quad \theta \in \Theta, \tag{2}$$

where $\nu_\theta(k,t) = \mu_\theta(k,t) + \beta(k,t)$, and η_k and σ_k denote respectively the mean and standard deviation of the Gaussian random variable used to model the additive readout noise at the k^{th} pixel.

In the context of the 3D resolution problem, we have for the scalar unknown parameter $\theta = d$. The intensity function of the inhomogeneous Poisson process is given by $\Lambda(\tau) = \Lambda_1(\tau) + \Lambda_2(\tau)$, $\tau \geq t_0$, where Λ_1 and Λ_2 are the photon detection rates of the two single molecules. The density function of the random variables modeling the spatial coordinates is given by

$$f_{d,\tau}(r) = \frac{\epsilon_1(\tau)}{M^2} q_{z_{01}(d),1}\left(\frac{x}{M} - x_{01}(d), \frac{y}{M} - y_{01}(d)\right) + \frac{\epsilon_2(\tau)}{M^2} q_{z_{02}(d),2}\left(\frac{x}{M} - x_{02}(d), \frac{y}{M} - y_{02}(d)\right), \tag{3}$$

where $r = (x,y) \in \mathbb{R}^2$, $\epsilon_i(\tau) = \Lambda_i(\tau)/(\Lambda_1(\tau) + \Lambda_2(\tau))$, $i = 1, 2$, $\tau \geq t_0$, M is the magnification of the imaging setup, (x_{01}, y_{01}, z_{01}) and (x_{02}, y_{02}, z_{02}) are the 3D spatial coordinates of the two single molecules, and $q_{z_{01}(d),1}$ and $q_{z_{02}(d),2}$ are the image functions of the two single molecules. By definition, an image function q_{z_0} is the image of an object at unit magnification when the object is located at $(0, 0, z_0)$, $z_0 \in \mathbb{R}$, in the object space.[6]

As illustrated in Fig. 2, which is an extension of the depiction of the single molecule pair in Fig. 1, the spatial coordinates of each single molecule can be given as functions of the separation distance d, and in terms of the midpoint coordinates (s_x, s_y, s_z) and the orientation angles ω and ϕ of the line segment P_1P_2 joining the two single molecules. With respect to focal plane 1 (see Fig. 1), we have, for single molecule P_1, $x_{01}(d) = s_x + \frac{d\sin\omega}{2}\cos\phi$, $y_{01}(d) = s_y + \frac{d\sin\omega}{2}\sin\phi$, and $z_{01}(d) = s_z + \frac{d}{2}\cos\omega$, and similarly, for single molecule P_2, $x_{02}(d) = s_x - \frac{d\sin\omega}{2}\cos\phi$, $y_{02}(d) = s_y - \frac{d\sin\omega}{2}\sin\phi$, and $z_{02}(d) = s_z - \frac{d}{2}\cos\omega$.

For a conventional single focal plane microscope setup that images focal plane 1, the 3D resolution measure is the square root of the inverse of the Fisher information matrix presented up to this point. To extend the result to a two-plane imaging setup, we make use of the assumption that in a multifocal plane setup, the image data acquired from each focal plane is represented by an independent image detection process. As a consequence, the Fisher information matrix for the entire multifocal plane setup is just the sum of the Fisher information matrices for image data captured from the individual focal planes. For a two-plane imaging setup, the Fisher information matrix $\mathbf{I}_{tot}(d)$ is then given by

$$\mathbf{I}_{tot}(d) = \mathbf{I}_{plane1}(d) + \mathbf{I}_{plane2}(d), \tag{4}$$

where $\mathbf{I}_{plane1}(d)$ and $\mathbf{I}_{plane2}(d)$ are the Fisher information matrices for the image data captured from the two focal planes. The expression for $\mathbf{I}_{plane2}(d)$ will be the same as the expression for $\mathbf{I}_{plane1}(d)$, but with two exceptions. First, s_z will be substituted by $s_z - \Delta z_f$, where Δz_f is the distance between the two focal planes (see Fig. 1), so that the axial coordinates $z_{01}(d)$ and $z_{02}(d)$ are given with respect to focal plane 2. Second, a different magnification will be associated with focal plane 2. The 3D resolution measure for a two-plane imaging setup is, by definition, the square root of $\mathbf{I}_{tot}^{-1}(d)$.

4. RESULTS

In all results that follow, the two single molecules are assumed to have equal and constant photon detection rate Λ_0, i.e., $\Lambda_1(\tau) = \Lambda_2(\tau) = \Lambda_0$, $\tau \geq t_0$. Moreover, the same image function q_{z_0} is assumed for the two single molecules, i.e., $q_{z_0,1}(x,y) = q_{z_0,2}(x,y) = q_{z_0}(x,y)$, $(x,y) \in \mathbb{R}^2$, $z_0 \in \mathbb{R}$, and is given by the scalar diffraction-based 3D point spread function[8]

$$q_{z_0}(x,y) = \frac{\left|\int_0^1 J_0\left(ka\rho\frac{\sqrt{x^2+y^2}}{z_d}\right) e^{jW_{z_0}(\rho)}\rho d\rho\right|^2}{\int_{\mathbb{R}^2}\left|\int_0^1 J_0\left(ka\rho\frac{\sqrt{x^2+y^2}}{z_d}\right) e^{jW_{z_0}(\rho)}\rho d\rho\right|^2 dxdy}, \tag{5}$$

where (x,y) is an arbitrary point on the detector plane, z_d is the axial distance between the detector plane and the back focal plane of the microscope lens system, $k = 2\pi/\lambda$, where λ is the wavelength of the detected photons, a is the radius of the limiting aperture of the microscope projected onto the back focal plane of the lens system, J_0 is the zeroth order Bessel function of the first kind, and W_{z_0} is the phase aberration term. The

phase aberration used corresponds to that of the classical 3D point spread function model of Born and Wolf,[9] and is given by

$$W_{z_0}(\rho) = \frac{\pi(NA)^2 z_0}{n_{oil}\lambda}\rho^2, \quad \rho \in (0,1), \quad z_0 \in \mathbb{R}, \tag{6}$$

where NA denotes the numerical aperture of the microscope objective and n_{oil} denotes the immersion oil refractive index.

The two single molecules are assumed to lie in the xz plane, i.e., the angle $\phi = 0$, and the midpoint of the line segment joining them is positioned at the center of a 21×21 pixel array with a pixel dimension of 13 $\mu m \times$ 13 μm. The wavelength of the detected photons is set to $\lambda = 520$ nm, the image acquisition time is set to $t = 1$ s (with $t_0 = 0$ s), the numerical aperture of the microscope objective is set to $NA = 1.45$, and the refractive index of the immersion oil is set to $n_{oil} = 1.515$.

For the two-plane imaging setup, a plane spacing of $\Delta z_f = 500$ nm (see Fig. 1) is assumed. The magnification is set to 100 for focal plane 1 and 97.98 for focal plane 2. The latter magnification value is obtained based on the 500 nm plane spacing in the object space using geometrical optics. The total fluorescence collected by the microscope objective is assumed to be split equally into two light paths. The constant photon detection rate is set to $\Lambda_0 = 2500$ photons/s per single molecule per focal plane. When noise due to cellular autofluorescence, scattering, etc. is considered, for each focal plane the mean of the additive Poisson noise is set to 80 photons/pixel/s for all pixels.

The conventional single-plane imaging setup that is compared with the two-plane setup is assumed to be one that consists of focal plane 1. Since in this case the collected fluorescence is not divided between light paths, the photon detection rate is twice that for the two-plane setup and is set to 5000 photons/s per single molecule. For the same reason, when noise due to spurious sources is taken into account, the mean of the additive Poisson noise is set to twice that for the two-plane setup, i.e., to 160 photons/pixel/s for all pixels.

When noise due to the detector readout process is considered, for any focal plane the mean and standard deviation of the additive Gaussian noise are set to 0 e^- per pixel and 8 e^- per pixel, respectively, for all pixels.

All results are presented with the 3D resolution measure plotted as a function of the axial distance from focal plane 1 of the midpoint of the line segment joining the two single molecules, i.e., as a function of s_z (see Fig. 1).

4.1 Dependence on axial location

From Fig. 3 and Fig. 4, which show the 3D resolution measure for the two-plane imaging setup for various separation distances and spatial orientations of the single molecule pair, we see that a symmetry about the midpoint between the two focal planes (i.e., about axial location $s_z = \Delta z_f/2 = 250$ nm) is exhibited by the resolution measure. This symmetry, however, is not exact. Because of the different magnifications associated with the two focal planes, the resolution measure for a single molecule pair centered at $s_z = \Delta z_f/2 + \Delta z$ is only close to, but not identical to that at $s_z = \Delta z_f/2 - \Delta z$, for all $\Delta z > 0$.

4.2 Dependence on separation distance

Fig. 3 shows the 3D resolution measure for the two-plane imaging setup for four different distances of separation d between the two single molecules. Here the spatial orientation of the single molecule pair is such that the line segment joining them forms a 45° angle with the positive z axis, i.e., the angle $\omega = \pi/4$. Regardless of the value of d, we see that the resolution measure stays relatively flat in the one-micron interval from $s_z = \Delta z_f/2 - \Delta z_f = -250$ nm to $s_z = \Delta z_f/2 + \Delta z_f = 750$ nm. Outside of this flat interval, the resolution measure undergoes considerably more deterioration as the single molecule pair is moved along the optical axis in either direction away from the two focal planes.

For a given axial location s_z of the single molecule pair, the accuracy with which the separation distance can be resolved consistently worsens as the separation distance decreases. For values of s_z in the flat one-micron interval, good accuracy in the range of ± 5.6 nm to ± 7.9 nm (± 15.9 nm to ± 22.8 nm) is predicted by the resolution measure for resolving a separation distance of 200 nm (50 nm). However, poor accuracy in the range of ± 38.9 nm to ± 55.9 nm (± 77.5 nm to ± 111.5 nm) is predicted for resolving a small separation distance of 20 nm (10 nm). It is important to note, however, that by increasing the number of detected photons from the single molecules, the accuracy for the small distances can be improved to more tolerable levels.

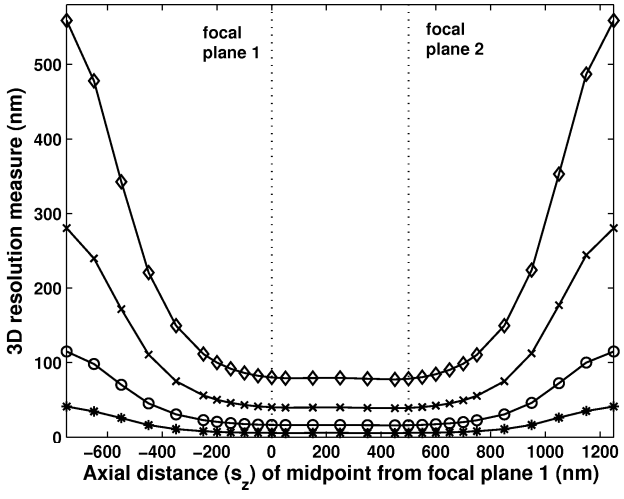

Figure 3. Comparison of two-plane 3D resolution measure for pixelated detectors in the presence of additive Poisson and additive Gaussian noise sources for separation distances of $d = 10$ nm ($\diamond$), $d = 20$ nm ($\times$), $d = 50$ nm ($\circ$), and $d = 200$ nm ($*$). The two-plane imaging setup has a focal plane spacing of $\Delta z_f = 500$ nm. The magnification for focal plane 1 is set to 100, and that for focal plane 2 is set to 97.98. The orientation angles are set to $\phi = 0$ and $\omega = \pi/4$, such that the line segment joining the two single molecules lies in the xz plane and forms a 45° angle with the positive z axis. The midpoint of the line segment joining the two molecules is placed at the center of a 21×21 pixel array with a pixel size of $13\ \mu m \times 13\ \mu m$. The wavelength of the detected photons is set to $\lambda = 520$ nm, the image acquisition time is set to $t = 1$ s, the numerical aperture of the microscope objective is set to $NA = 1.45$, and the refractive index of the immersion oil is set to $n_{oil} = 1.515$. The photon detection rate is set to $\Lambda_0 = 2500$ photons/s per single molecule per focal plane. For each focal plane, the mean of the additive Poisson noise is set to 80 photons/pixel/s for all pixels, and the mean and standard deviation of the additive Gaussian noise are set to 0 e^- per pixel and 8 e^- per pixel, respectively, for all pixels.

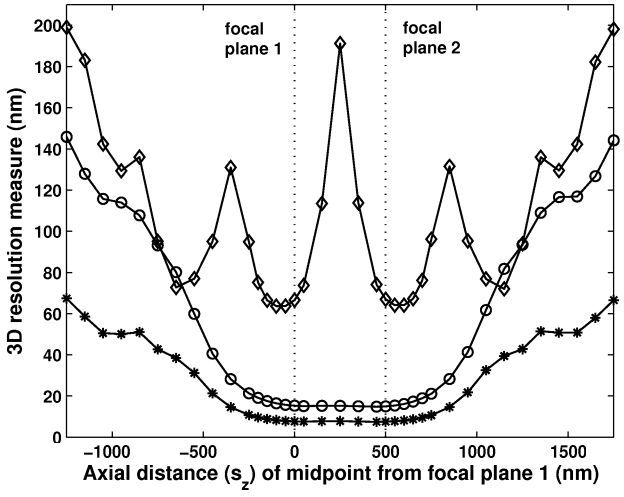

Figure 4. Comparison of two-plane 3D resolution measure for pixelated detectors in the presence of additive Poisson noise for orientation angles of $\omega = \pi/2$ ($*$), $\omega = \pi/4$ ($\circ$), and $\omega = 0$ ($\diamond$). The value of ω is the angle that the line segment joining the two single molecules forms with the positive z axis. The other orientation angle is set to $\phi = 0$ such that the two single molecules lie in the xz plane. The separation distance between the two single molecules is set to $d = 50$ nm. Numerical values of all other parameters are as given in Fig. 3, with the exception that here no additive Gaussian noise is present.

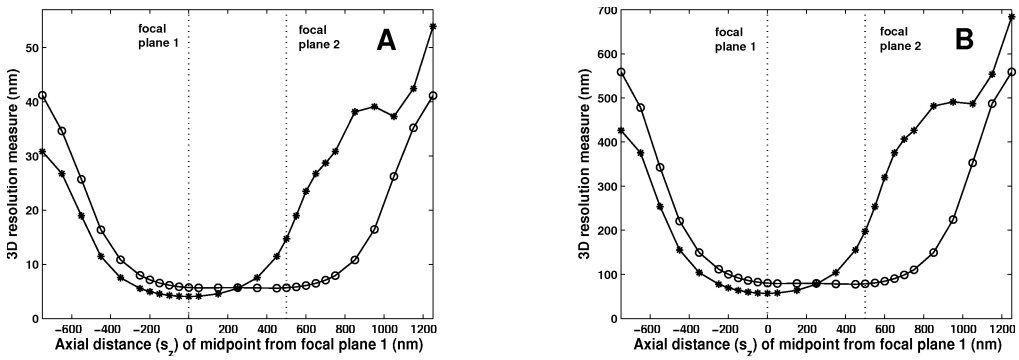

Figure 5. Comparison of two-plane ($\circ$) and conventional single-plane ($*$) 3D resolution measures for pixelated detectors in the presence of additive Poisson and additive Gaussian noise sources. Plots are shown for separation distances of $d = 200$ nm (A) and $d = 10$ nm (B). The orientation angles are set to $\phi = 0$ and $\omega = \pi/4$, such that the line segment joining the two single molecules lies in the xz plane and forms a 45° angle with the positive z axis. For the two-plane imaging setup, numerical values of all other parameters are as given in Fig. 3. The conventional single-plane setup is one that consists of focal plane 1. For the single-plane setup, the magnification is set to 100, the photon detection rate is set to $\Lambda_0 = 5000$ photons/s per single molecule, the mean of the additive Poisson noise is set to 160 photons/pixel/s for all pixels, and the mean and standard deviation of the additive Gaussian noise are set to 0 e^- per pixel and 8 e^- per pixel, respectively, for all pixels. Numerical values of all other parameters are identical to those used for the two-plane setup.

4.3 Dependence on spatial orientation

Fig. 4 shows the effect of the spatial orientation of the single molecule pair on the 3D resolution measure for the two-plane imaging setup. Plots are shown for three different values of the orientation angle ω (see Fig. 2): $\pi/2$, which corresponds to the two single molecules lying perpendicular to the optical axis, $\pi/4$, which corresponds to the line segment joining the two single molecules forming a 45° angle with the positive z axis, and 0, which corresponds to the two single molecules lying parallel to the optical axis. The two single molecules are 50 nm apart. For any given axial location s_z of the single molecule pair, the numerical value of the resolution measure is consistently higher for $\omega = \pi/4$ and $\omega = 0$ than for $\omega = \pi/2$. This is not unexpected since an optical microscope is well known to suffer from poor depth discrimination and hence is better at resolving the distance between two point sources that lie in a plane perpendicular to the optical axis (i.e., when $\omega = \pi/2$). In the relatively flat one-micron interval from $s_z = -250$ nm to $s_z = 750$ nm, an accuracy in the range of ± 7.4 nm to ± 10.7 nm is predicted to resolve the 50 nm separation distance for $\omega = \pi/2$, but for $\omega = \pi/4$, the predicted accuracy deteriorates approximately two-fold to the range of ± 14.8 nm to ± 21.2 nm. For $\omega = 0$, the predicted accuracy becomes significantly worse and can be no better than ± 63.6 nm in the entire one-micron interval. Note that the general shape of the curve for $\omega = 0$ is distinct from that of the other two orientations.

4.4 Two-plane setup vs. conventional single-plane setup

Fig. 5 compares the 3D resolution measure for the two-plane imaging setup with that for a comparable conventional single-plane setup. Here the orientation angle $\omega = \pi/4$, meaning that the line segment joining the two single molecules forms a 45° angle with the positive z axis. Plots are shown for separation distances of 200 nm (panel A) and 10 nm (panel B). We see that for both separation distances, symmetry is exhibited by the single-plane resolution measure about $s_z = 0$, which corresponds to the axial location of focal plane 1, the plane of focus of the conventional single-plane setup.

For either distance of separation, the single-plane setup provides better accuracy in resolving the distance than the two-plane setup when the midpoint of the line segment joining the two single molecules is positioned closer to the focal plane of the single-plane setup, i.e., focal plane 1, or placed exactly at the midpoint between focal plane 1 and focal plane 2. More precisely, the single-plane setup gives better performance for axial locations $s_z \leq \Delta z_f/2 = 250$ nm. In contrast, when the single molecule pair is situated closer to focal plane 2, i.e., for $s_z > 250$ nm, it is the two-plane setup that outperforms the single-plane setup. Importantly, significant

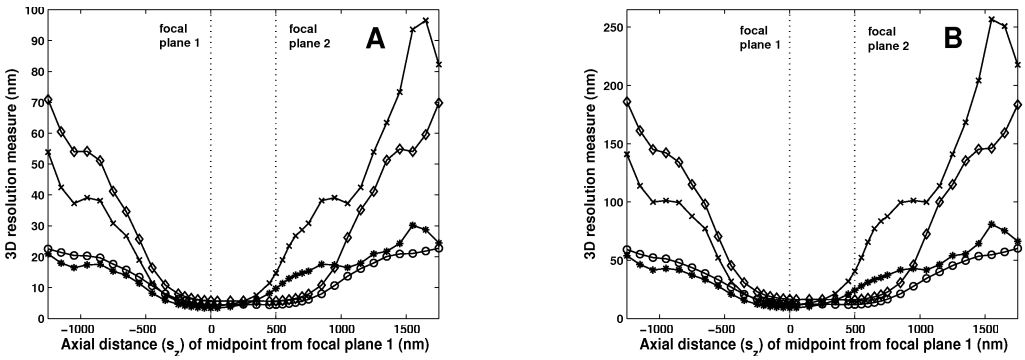

Figure 6. Comparison of the effect of noise on the two-plane and conventional single-plane 3D resolution measures for pixelated detectors. Resolution measures are evaluated for the two-plane setup and the single-plane setup in the absence of noise sources ($\circ$ two-plane, $*$ single-plane) and in the presence of additive Poisson and additive Gaussian noise sources ($\diamond$ two-plane, $\times$ single-plane). In the scenario with noise sources, the numbers used are as follows. For the two-plane setup, for each focal plane the mean of the additive Poisson noise is set to 80 photons/pixel/s for all pixels. For the single-plane setup, the mean of the additive Poisson noise is set to 160 photons/pixel/s for all pixels. In both setups, the mean and standard deviation of the additive Gaussian noise for a given focal plane are set to 0 e^- per pixel and 8 e^- per pixel, respectively, for all pixels. Plots are shown for separation distances of $d = 200$ nm (A) and $d = 50$ nm (B). The orientation angles are set to $\phi = 0$ and $\omega = \pi/4$, such that the line segment joining the two single molecules lies in the xz plane and forms a 45° angle with the positive z axis. Numerical values of all other parameters are as given in Fig. 3 for the two-plane setup, and as given in Fig. 5 for the single-plane setup.

improvement in the accuracy is obtained with the two-plane setup in the interval from $s_z = 250$ nm to $s_z = 750$ nm, within which the two-plane resolution measure remains relatively flat compared to the single-plane resolution measure. In that interval, a separation distance of 200 nm (10 nm) can be resolved with the two-plane setup with an accuracy in the range of ± 5.6 nm to ± 7.9 nm (± 77.5 nm to ± 110.4 nm), as opposed to ± 5.5 nm to ± 30.8 nm (± 77.5 nm to ± 426.2 nm) with the single-plane setup. Though here the accuracy for the 10 nm separation distance is unacceptably poor using either imaging setup, it must be noted that more reasonable levels of accuracy are attainable if more photons are collected from the single molecule pair.

4.5 Effect of noise

Fig. 6 compares the effect of noise on the 3D resolution measure for the two-plane imaging setup and the conventional single-plane setup. Two different noise levels are considered for each setup, one where no noise of any kind is assumed, and one where additive Poisson (e.g., due to cellular autofluorescence, scattering) and additive Gaussian (i.e., due to detector readout process) noise sources are assumed. In the scenario with noise sources, the mean of the additive Poisson noise is set to 80 photons/pixel/s for all pixels for each focal plane of the two-plane setup, and 160 photons/pixel/s for the single-plane setup. In both setups, the mean and standard deviation of the additive Gaussian noise for a given focal plane are set to 0 e^- per pixel and 8 e^- per pixel, respectively, for all pixels. The spatial orientation of the single molecule pair is one where the line segment joining them forms a 45° angle with the positive z axis, i.e., the angle $\omega = \pi/4$. The comparison is made for two different separation distances: 200 nm (panel A) and 50 nm (panel B).

Similar patterns are observed for both separation distances. In general, for a given axial location s_z of the single molecule pair, the introduction of noise causes a deterioration of the accuracy with which the separation distance can be resolved in both imaging setups. Roughly speaking, for a given value of s_z, the deterioration in one setup is mirrored by a deterioration of comparable level in the other setup. Exception to this general behavior is seen for axial locations in the range of $s_z = 250$ nm to $s_z = 750$ nm. Whereas the two-plane resolution measure experiences little deterioration and remains relatively flat throughout this interval when noise is introduced, the single-plane resolution measure undergoes a much more significant deterioration. In that interval, a separation distance of 200 nm (50 nm) is predicted to be resolvable with the two-plane setup with an accuracy in the range of ± 4.4 nm to ± 6.1 nm (± 11.7 nm to ± 16.5 nm) in the absence of noise. When noise is introduced, the two-plane

resolution measure deteriorates only slightly to the range of ±5.6 nm to ±7.9 nm (±15.9 nm to ±22.6 nm) for a separation distance of 200 nm (50 nm). In contrast, in the same interval a separation distance of 200 nm (50 nm) can be resolved with the single-plane setup with an accuracy in the range of ±4.5 nm to ±15.3 nm (±12.1 nm to ±37.1 nm) in the absence of noise. When noise is introduced, however, the single-plane resolution measure worsens considerably to the range of ±5.5 nm to ±30.8 nm (±15.9 nm to ±87.6 nm) for a separation distance of 200 nm (50 nm).

ACKNOWLEDGMENTS

This research was supported in part by the National Institutes of Health (R01 GM071048).

REFERENCES

1. S. Ram, E. S. Ward, and R. J. Ober, "Beyond Rayleigh's criterion: A resolution measure with application to single-molecule microscopy," *PNAS* **103**(12), pp. 4457–4462, 2006.
2. S. Ram, A. V. Abraham, E. S. Ward, and R. J. Ober, "A novel 3D resolution measure for optical microscopes with applications to single molecule imaging," *Proc. of SPIE* **6444**, pp. 64440D1–D9, 2007.
3. P. Prabhat, S. Ram, E. S. Ward, and R. J. Ober, "Simultaneous imaging of different focal planes in fluorescence microscopy for the study of cellular dynamics in three dimensions," *IEEE Trans. Nanobioscience* **3**, pp. 237–242, 2004.
4. S. Ram, J. Chao, P. Prabhat, E. S. Ward, and R. J. Ober, "A novel approach to determining the three-dimensional location of microscopic objects with applications to 3D particle tracking," *Proc. of SPIE* **6443**, pp. 64430D1–D7, 2007.
5. P. Prabhat, Z. Gan, J. Chao, S. Ram, C. Vaccaro, S. Gibbons, R. J. Ober, and E. S. Ward, "Elucidation of intracellular recycling pathways leading to exocytosis of the Fc receptor, FcRn, by using multifocal plane microscopy," *PNAS* **104**, pp. 5889–5894, 2007.
6. S. Ram, E. S. Ward, and R. J. Ober, "A stochastic analysis of performance limits for optical microscopes," *Multidim. Syst. Sig. Process.* **17**, pp. 27–57, 2006.
7. D. L. Snyder and M. I. Miller, *Random point processes in time and space.*, Springer Verlag, New York, USA, 2nd ed., 1991.
8. S. F. F. Gibson, *Modeling the 3D imaging properties of the fluorescence light microscope.* PhD thesis, Carnegie-Mellon University, 1990.
9. M. Born and E. Wolf, *Principles of Optics*, Cambridge University Press, Cambridge, UK, 1999.